Available online at www.sciencedirect.com
ScienceDirect
Journal of Power Sources 160 (2006) 548–557
JOURNAL OF POWER SOURCES
www.elsevier.com/locate/jpowsour

Passive film formation on a graphite electrode: Effect of siloxane structures

Hiroshi Nakahara [a,*], Sang-Young Yoon [a], Steven Nutt [b]

[a] *Quallion LLC, Sylmar Biomedical Park, 12744 San Fernando Rd., Sylmar, CA 91342, USA*
[b] *Department of Materials Science and Engineering, University of Southern California, Los Angeles, CA 90089-0241, USA*

Received 17 October 2005; received in revised form 24 December 2005; accepted 5 January 2006
Available online 3 February 2006

Abstract

Passive films on highly oriented pyrolytic graphite (HOPG) lithiated in siloxane-based electrolytes were investigated. Microanalysis and electrochemical impedance spectroscopy (EIS) were employed to understand the effects of siloxane molecular structure on film morphology and electrochemical properties. In the experiments, the numbers of silicon and ethylene oxide (EO) side chain groups on the siloxane molecule were varied, and a methylene group was also attached. The morphological and electrochemical properties of the passive film depended strongly on the siloxane molecule structure. The surface morphology of the passive film was similar to films formed in a carbonate electrolyte. However, after lithiation in a siloxane-based electrolyte having two silicones, one EO group, and a spacer group (named 2SM3), no gel-like film was formed. The silicon and oxygen concentrations on HOPG edge planes were greater than on the basal plane, and were reduced for the electrolyte with the 2SM3 spacer group. Conductivity decreased in the range of 1.7–2.0 V for all electrolytes. The film resistance and the charge transfer resistance of 2SM3 were the most constant over 0–0.5 V, the practical potential range for graphite electrodes in lithium secondary batteries. The results indicate that 2SM3 was well-suited for use as an electrolyte for lithium batteries.

Keywords: Lithium battery; Graphite; Siloxane molecular structure; LiBOB; Passive film

1. Introduction

Considerable research has been devoted to the formation of the solid electrolyte interface (SEI) on the graphite electrode surface in non-aqueous electrolytes, such as the ethylene carbonate/diethyl carbonate system [1,2]. Exfoliation of graphene layers reportedly occurs during initial charging in propylene carbonate-based electrolytes because of co-intercalation of solvent [1,3]. Earlier studies asserted that the SEI film formed mainly by a solvent decomposition reaction, and that it was composed of $ROCO_2Li$ species, Li_2CO_3, and LiF [4–7]. Investigators subsequently concluded that the novel lithium salt, lithium bis(oxalato) borate (LiBOB), resulted in an SEI film that formed directly on graphite, rather than by a solvent decomposition reaction [8–10].

Polysiloxane-based electrolyte is a suitable candidate electrolyte for lithium battery systems because of the high conductivity relative to other polymer materials [11–15]. Polyethylene oxide (PEO) is a well-known solid polymer electrolyte that shows conductivity in the range of 10^{-6} to 10^{-7} S cm^{-1} [11–15]. By comparison, the conductivity of polysiloxane-based electrolyte exceeds a value of approximately 10^{-3} S cm^{-1} [16]. Polysiloxane-based electrolyte has emerged as a primary candidate for the development of large lithium batteries for applications such as electric vehicles, in which safety is a prime consideration [16].

SEI formation on graphite surfaces in a polysiloxane-based electrolyte has been investigated in recent reports [17–20]. In one report, the existence of two types of passive film and the associated morphological features was revealed by SEM observations [17,18]. One passive film was island-like and formed directly on the graphite surface, while the other was gel-like film and covered the island-like film [17,18].

Electrochemical impedance spectroscopy (EIS) is a powerful tool to investigate electrolyte–electrode interface reactions [21–29]. For example, EIS has been used to analyze the electrochemical lithium intercalation reaction into carbonaceous material in the carbonate electrolyte system and the subsequent

* Corresponding author. Tel.: +1 818 833 2000; fax: +1 818 833 2001.
E-mail address: hiroshi@quallion.com (H. Nakahara).

0378-7753/$ – see front matter © 2006 Elsevier B.V. All rights reserved.
doi:10.1016/j.jpowsour.2006.01.013

formation of a SEI film [30–36]. EIS has also been performed on graphite/lithium cells with polysiloxane-based electrolyte containing LiBOB. The spectra revealed that the electrochemical characteristics of the passive films, such as film resistance and charge transfer resistance, depended on cell voltage, and that the magnitudes of these parameters were much greater than those of conventional carbonate-based electrolytes [18–20].

Recent investigations have focused on modifications to improve lithium batteries. For instance, the addition of VEC to the polysiloxane-based electrolyte increased the discharge capacity of the graphite electrode and inhibited gel-like film formation, resulting in a decrease in film resistance and charge transfer resistance [17,19]. In similar fashion, the type of electrolyte salt also affected passive film formation and the electrochemical response of the passive films on graphite electrodes [20]. These reports indicated that the electrochemical and morphological characteristics of passive films that form on the graphite electrode surface (when charged in a polysiloxane-based electrolyte) could be modified by optimizing the electrolyte. Electrolyte optimization is thus a promising path to commercialization.

Electrolyte solvents have been used to modify the passive films on graphite electrodes [37–42]. The expected functions and characteristics of the electrolyte solvents selected were: (a) to dissolve an electrolyte salt with sufficient concentration, (b) to provide sufficient ion transport, (c) inert to all cell components, (d) liquid or solid state in the utilized temperature range, and (e) safe (high flash point, non-toxic) and economical. Investigation of the chosen non-aqueous solvents, such as carbonates and ethers, revealed that the mechanism of passive film formation depended on the type of molecular structure in the solvent, such as polypropylene carbonate and ethylene carbonate [1–3,7,42].

In this study, various polysiloxane-based electrolytes containing LiBOB were used to investigate the effect of siloxane molecule structures on the formation of passive films on the graphite electrode. Eight types of siloxane molecule were used. The number of silicons (1, 2, or 10) and the number of ethylene oxide (EO) side chain groups (1, 2, or 8) in a siloxane molecular were varied. The effect of a methylene group (called a spacer group) inserted between an oxygen attached to the silicon backbone and an EO was investigated. The surface morphology of highly oriented pyrolytic graphite (HOPG) was examined after charging in the polysiloxane-based electrolyte containing dissolved LiBOB, and the composition of the passive films was measured. EIS was performed to assess the change in electrochemical characteristics of the passive films.

2. Experimental

2.1. Siloxane synthesis methods

Siloxanes having eight different molecular structures were prepared for study. All siloxane liquids were synthesized and provided at the University of Wisconsin. The molecular structures were confirmed by FT-IR and NMR analyses. No impurities were detectable in the siloxanes by FT-IR and NMR analyses. The siloxane molecular structures, the number of silicons, the number of EO groups, and the presence of spacer groups are shown in Table 1. A nomenclature was employed in which, for example, the siloxane comprised of 10 silicons, 8 EO group side chains, and absence of spacer group was named W100. The synthesis methods used to prepare 3 of the siloxanes (with 10 or 2 silicons in the molecule) are described below. Similar methods were employed to synthesize the other siloxanes having one silicon [43].

A dehydrogenation reaction was carried out to generate the siloxanes having 10 or 2 silicons in the molecule. Tri(ethylene glycol) allyl methyl ether with polymethylhydrosiloxane (Gelest) and toluene (distilled over Na and benzophenone prior to use) were added to a flame-dried schlenk flask under nitrogen atmosphere. To this solution, tri(pentafluorophenyl) borane ($B(C_6F_5)_3$, 0.05 mol% of Si–H) in toluene was added. The reaction mixture was heated to 75–80 °C and vigorously stirred. Bubbling was observed. Aliquots were taken periodically and the dehydrogenative coupling reaction was monitored by FT-IR. After the reaction was complete, excess tri(ethylene glycol) methyl ether and the solvent were removed by Kugelrohr distillation. The result was purified by performing two sequential vacuum distillations using a central fraction of the distillate as the product of each distillation.

For siloxanes having one silicon in the molecule, a dehydrogenation reaction was performed to generate a silane. Tri(ethylene glycol) methyl ether (vacuum distilled prior to use), triethylamine (Aldrich), and anhydrous THF (Aldrich) were syringed into a flask which was placed in an ice water bath. The resulting solution was stirred and distilled, and dimethyldichlorosilane (for 1ND3) or trimethylchlorosilane (for 1NM3 and 1S3M3) was added to the solution. After adding the dimethyldichlorosilane, or trimethylchlorosilane, the mixture was stirred at room temperature for an additional 2 h and then warmed to 50 °C and filtered to separate a white solid from a solution that included the silane. The solvent was removed from the solution under reduced pressure to yield a crude product. The crude product was purified by fractional distillation and its structure was confirmed spectroscopically.

2.2. SEM observation and EDX analysis

Each siloxane shown in Table 1 was used as an electrolyte and contained LiBOB (Chemetall GmbH), dissolved to achieve a 0.8 M concentration, and each was a liquid at room temperature. A block of HOPG (2 mm × 2 mm × 1 mm) was used for the working electrode. Copper mesh was used as a current collector, and was sandwiched around the HOPG block electrode. The electrode was covered with a polyethylene porous separator, and lithium metal was pressed against a copper mesh and used as the counter electrode. The working electrode, counter electrode, separator, and electrolyte, were packaged in an aluminum laminated bag that was heat-sealed. The laminated cell was charged to 0.02 V. The charged electrode was removed from the disassembled cell in a glove box filled with Ar gas and a dew-point maintained below −75 °C, rinsed with diethyl carbonate (DEC), and dried under vacuum at room temperature. The surfaces of the HOPG were examined by SEM (JEOL JSM-5910LV) after a

Table 1
Molecular structure of siloxane (ethylene oxide)

Code name	Molecular structure	Number of Si	Number of PEO side chain	Spacer –(CH_2)–
W100	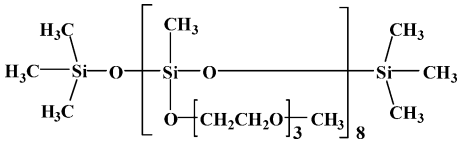	10	8	No
2ND3	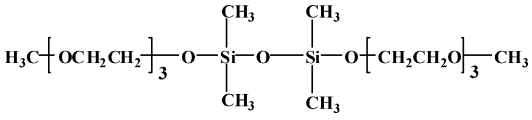	2	2	No
1ND3	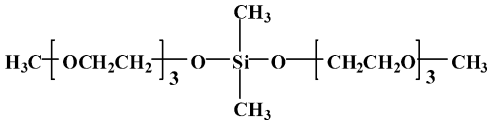	1	2	No
1NM3	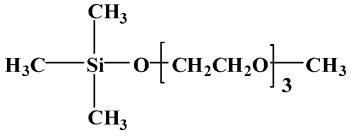	1	1	No
2SM3	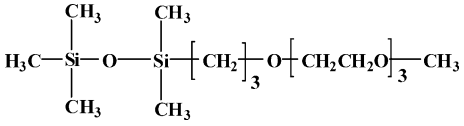	2	1	Yes
1S3M3	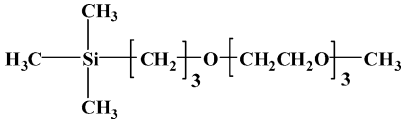	1	1	Yes

gold sputtering coat. In addition, the composition of the surface films on the specimens was analyzed by energy dispersive X-ray spectroscopy (EDS: Oxford Instruments, EDS INCAEnergy 7274).

2.3. Electrochemical impedance spectroscopy

Graphite electrodes were prepared by mixing 33.6 g of mesocarbon microbeads (Osaka Gas Co. Ltd., MCMB 25–28), 14.4 g of graphite fiber (Petoca Co. Ltd., GMCF), 62.6 g of 2 wt% aqueous solution of carboxymethyl cellulose (Dai-ichi Kogyo Seiyaku Co. Ltd., Celogen WSC), and 1.88 g of a 40% aqueous dispersion of styrene butadiene rubber (Dai-ichi Kogyo Seiyaku Co. Ltd., BM-400) in a mixer. The mixture was spread on a copper foil (10 μm thick) with a doctor blade and dried in an oven at 80 °C. The dried electrode plate was then pressed by using a roll press to a thickness of 102 μm. Pressed electrodes were dried in a vacuum oven at 120 °C for 12 h. The carbonaceous electrodes (15 mm in diameter) were punched out of the dried electrode plate. Lithium metal electrodes (16 mm in diameter) were punched from a lithium metal sheet (Honjo metal, 100 μm thick). Coin cells (2032-type) were prepared by stacking a lithium metal electrode, a separator, a carbonaceous electrode, spacer disks made from stainless steel, and a spring in sequence. The separator was a 25 μm-thick polyethylene porous membrane (Tonen Chemical Co. Ltd.). The separators and electrodes were immersed into each different siloxane-based electrolyte mentioned above. All parts used for the coin cell assembly were dried in a vacuum oven at 60 °C for more than 8 h.

AC impedance measurements were performed with a potentiostat (Solartron, SI1287) and a transfer function analyzer (Solartron, 1255B). The frequency used for the impedance measurements was 50 mHz to 200 kHz, and the signal amplitude was 10 mV. Potential step coulometry was performed with an electrochemical interface (Solartron, SI1287). Impedance spectra were measured after the cell had been charged at a rate of *C*/200 to the prescribed voltage and maintained at that voltage for 24 h. The voltage was then stepped to the next potential, and the procedure was repeated. In this manner, the cell was charged from the initial open circuit voltage (OCV) down to 0.05 V at 25 °C. The counter electrode and the reference electrode were lithium metal.

The impedance data were analyzed using commercial software (Scribner Associates, Inc., Zview™) that included a batch fitting function. The function was used to perform fitting for multiple sets of impedance spectra step-by-step. In this method, initial values of the parameter were obtained from values fitted in the previous step. These values were obtained for a set of measured impedance spectra, from which a complex plane plot was generated at a higher voltage. Next, the fitted parameters generated in one step were used as initial values to fit the spectra

of the previous step. These procedures were repeated in successive steps until the values of the fit parameters converged [44]. The conductivity of electrolyte was calculated using the real part of the impedance obtained in the high-frequency region of the complex plane plot.

3. Implementation of equivalent circuit model

EIS data for lithium ion cells and lithium metal cells have been reported extensively [22–24,26,45]. In related work, logic diagrams and equivalent circuits (ECs) have been proposed for cells with a graphite/lithium metal configuration [46–51]. In most of these studies, an *R–C* parallel or *R*–CPE parallel circuit was used to describe the presence of a surface film layer on the electrode [46,48–52]. EC expresses the electric property of graphite electrode charged in polysiloxane-based electrolyte (Fig. 1) [18–20]. Segments include: (a) electric connection resistance and the electrolyte bulk resistance corresponding to the resistance at the highest frequencies, followed by (b) an *R–C* parallel circuit describing the SEI layer in the middle frequency region, and finally (c) an *R–C* parallel circuit for double layer capacitance and charge transfer reaction, including a Warburg diffusion term in the low-frequency region corresponding to lithium diffusion in the solid state [30,33,34,49,53].

In general, because semicircles often tend to be depressed in a complex plane plot due to electrode geometry, a constant phase element (CPE) is used in an EC for the porous electrode. The use of a CPE is justified because of the geometrical effect on

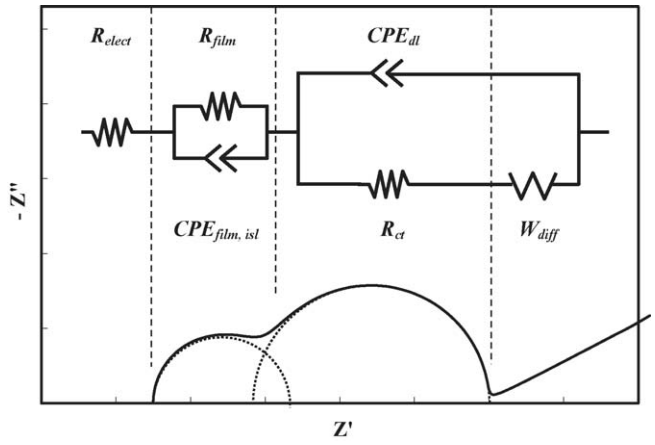

Fig. 1. Equivalent circuit for graphite/polysiloxane-based electrolyte/lithium metal cell.

capacitance in electrochemical reactions [54–57]. The complex impedance of a CPE, Z_{CPE}, is expressed by:

$$Z_{CPE} = \frac{1}{T \cdot (j \cdot \omega)^P} \quad (1)$$

where T represents the pseudo-capacitance that is modified by the electrode geometry, j an imaginary number, and P is an exponential parameter that expresses the electrode geometry as a number. Finally, $\omega = 2\pi f$ is the angular frequency and f is the frequency of the applied AC signal.

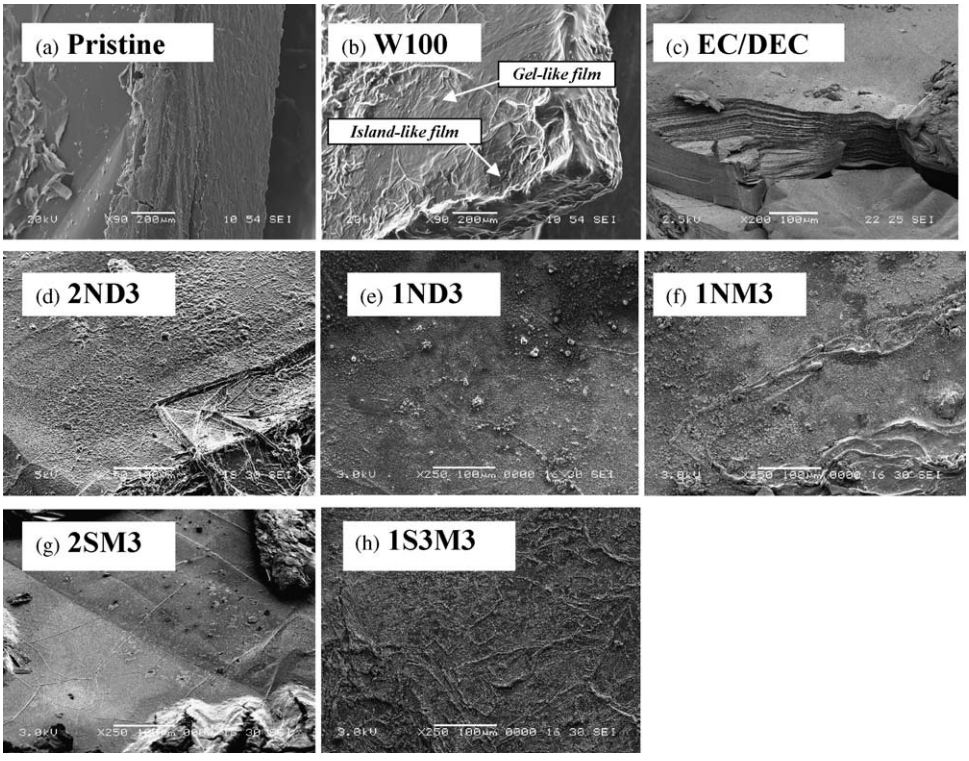

Fig. 2. SEM images of HOPG blocks charged at 0.02 V vs. Li/Li^+, after charging in various types of electrolyte containing LiBOB: (a) pristine; (b) W100; (c) EC/DEC; (d) 2ND3; (e) 1ND3; (f) 1NM3; (g) 2SM3; (h) 1S3M3.

In Fig. 1, the EC has the resistance element, R_{elect}, representing the resistance of the bulk electrolyte, and an R–CPE parallel circuit [45–50,58,59] for the passive film with resistance R_{film} and constant phase element, CPE_{film}. The final component is an R–CPE parallel [61] element that represents the electric double-layer capacitance as a constant-phase element, CPE_{dl}, and the charge transfer resistance, R_{ct}, representing the site where the electrochemical reaction occurs. Each CPE contains the pseudo-capacitance and exponential parameter, as expressed in Eq. (1), i.e., T_{film} and P_{film} for CPE_{film}, and T_{dl} and P_{dl} for CPE_{dl}, respectively. The diffusion impedance $W_{s,diff}$ is connected in series to R_{ct} [55,60,62–64].

4. Results

4.1. Microanalysis of films

SEM images of the HOPG blocks are shown in Fig. 2. The pristine HOPG exhibits clean edge planes and a basal plane (Fig. 2a). Using the W100 electrolyte, both island- and gel-like films are observed (Fig. 2b) [17,18]. The gel-like film covers the island-like film deposited on the HOPG surface, and the island-like film is exposed at sites where the gel-like film is ruptured (Fig. 2b) [17,18]. For comparison, an image of HOPG charged in a carbonate electrolyte is shown in Fig. 2c. An island-like film is apparent, but it is not as pronounced as that of W100. SEM images for 2ND3 (Fig. 2d), 1ND3 (Fig. 2e), 1NM3 (Fig. 2f), 2SM3 (Fig. 2g), and 1S3M3 (Fig. 2h) are also shown. None of these samples exhibited a gel-like film, but island-like films were present on the surface of HOPG for 2-Si and 1-Si siloxane molecule electrolytes.

Compositions of the surface films on the HOPG basal and edge planes were analyzed by EDS, the results of which are summarized in Table 2. For both basal and edge planes, only the W100 sample (without additive) showed significant concentrations of silicon. For all types of siloxane molecule, carbon was the primary element detected, and silicon concentrations on the basal planes were typically less than 0.6 at%. On edge planes, silicon concentrations were higher relative to those on the basal plane, a trend that was consistent for all siloxane molecules. In the W100 system, the concentration of silicon decreased with the addition of VEC [19].

Table 2
Atomic composition on the surface of HOPG lithiated in various siloxane electrolytes (EDX analysis result)

	Basal (at%)			Edge (at%)		
	C	O	Si	C	O	Si
W100	77.0	17.9	5.1	37.3	51.8	10.9
W100, VEC	85.7	14.3	0	33.3	64.8	1.9
2ND3	83.2	16.6	0.2	39.2	58.2	2.6
1ND3	69.8	30.0	0.2	42.1	57.3	0.6
1NM3	91.7	8.3	0	76.0	19.4	4.6
2SM3	96.6	3.3	0.1	79.4	18.9	1.7
1S3M3	90.2	9.2	0.6	77.8	19.7	2.5

4.2. EIS results

4.2.1. Complex plane plots and Bode plots

Fig. 3 shows EIS data plots measured at 0.5 V for samples W100, 2ND3, and 1ND3, all of which have no spacer group in the molecular structures but that have different numbers of silicon and EO side chain groups. Fig. 3a shows the

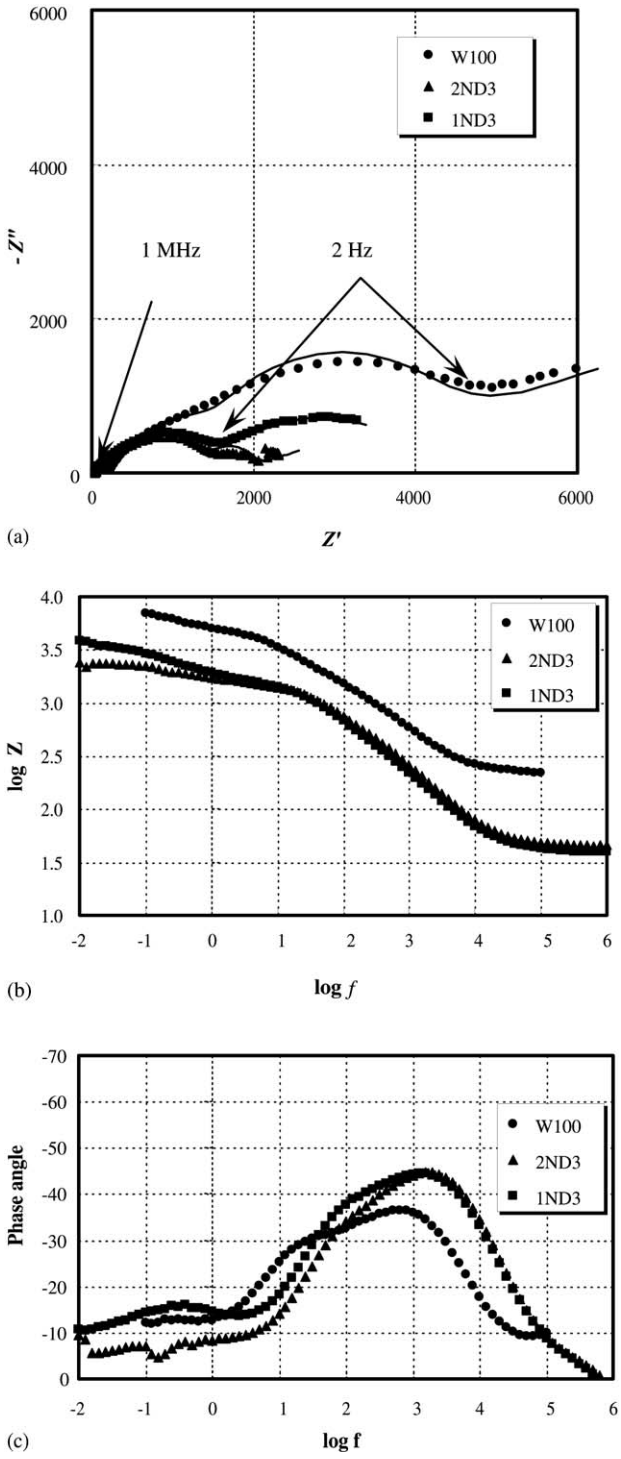

Fig. 3. (a–c) Nyquist plots and Bode plots for graphite/polysiloxane-based electrolyte/lithium metal cell measured at 0.5 V with various types of siloxane molecular structure having different number of Si.

complex plane plots, and Fig. 3b and c shows Bode plots. The semicircles in the complex plane plots are depressed and contain more than one semicircle. The semicircle in the middle- or low-frequency region became significantly broader as the cell voltage was decreased (not shown). As the applied voltage decreased, the straight line in the low frequency region became shorter, and an additional semicircle was detected (not shown). Fig. 3b shows the logarithm of the measured impedance modulus, $|Z|$, plotted against the logarithm of the applied frequency, and corresponds to the complex plane plots in Fig. 3a. The magnitude of the impedance modulus for W100 was greater than that for 2ND3 and 1ND3 in all frequency ranges. The magnitude of $|Z|$ for 2ND3 at less than 1 Hz was less than that for 1ND3. Fig. 3c shows the phase angle of the measured impedance plotted against the applied frequency. The phase angle increased with smaller numbers of silicon at 100 Hz.

The EIS data plots for 2ND3 and 2SM3 were measured at 0.5 V to elucidate the effect of a functional group (spacer group and EO side chain) on the impedance behavior. The functional group was attached to a silicon in the siloxane with two silicons. These plots are shown in Fig. 4, along with plots for 1ND3 and 1S3M3 with one silicon. Fig. 4a shows the complex plane plots, and Fig. 4b and c is Bode plots. The semicircle in the high- and middle-frequency range for 2SM3 was larger than that of the others (Fig. 4a). The plots for 2ND3 and 1ND3 (no spacer group) showed a second semicircle in the low-frequency range. The magnitude of the impedance modulus for the siloxane with spacer group and fewer EO side chains was greater than that without spacer and more EO side chains at frequencies below 10 Hz, and above 1000 Hz. The maximum phase angle for 2SM3 was observed at $10^{1.5}$ Hz, while the maximum for others occurred at $10^{3.1}$ Hz.

4.2.2. *Dependency of impedance elements in equivalent circuits on cell voltage*

All of the impedance elements of the EC depended on the cell voltage, for all the siloxane electrolytes tested. The conductivity of systems with W100, 2ND3, and 1ND3 (no spacer group) is plotted versus voltage (derived using the experimental value of R_{elect}) in Fig. 5a. The conductivity did not change significantly between 2.1 and 3.2 V, although it decreased sharply with a decrease in cell voltage between 1.6 and 1.9 V, and then more gradually in the range of 1.05–1.2 V. The magnitudes of conductivity for 2ND3 and 1ND3 were greater than that for W100. At voltages greater than 2 V, the conductivity for 1ND3 was greater than for 2ND3, while at voltages less than 1.8 V, the values were the same.

The conductivity of systems with 2ND3, 2SM3, 1ND3, and 1S3M3 is plotted in Fig. 5b. The magnitude of the conductivity drop for 2SM3 and 1S3M3, both of which contained a spacer group, was significantly lager than for 2ND3 and 1ND3 without spacer groups. The dependency of the system conductivity on cell voltage for 2SM3 and 1S3M3 showed a minimum at 1.6 and 1.7 V, respectively. The conductivity for 2SM3 was constant in the cell voltage range below 1.2 V. For 1S3M3, the conductivity increased with decreasing cell voltage.

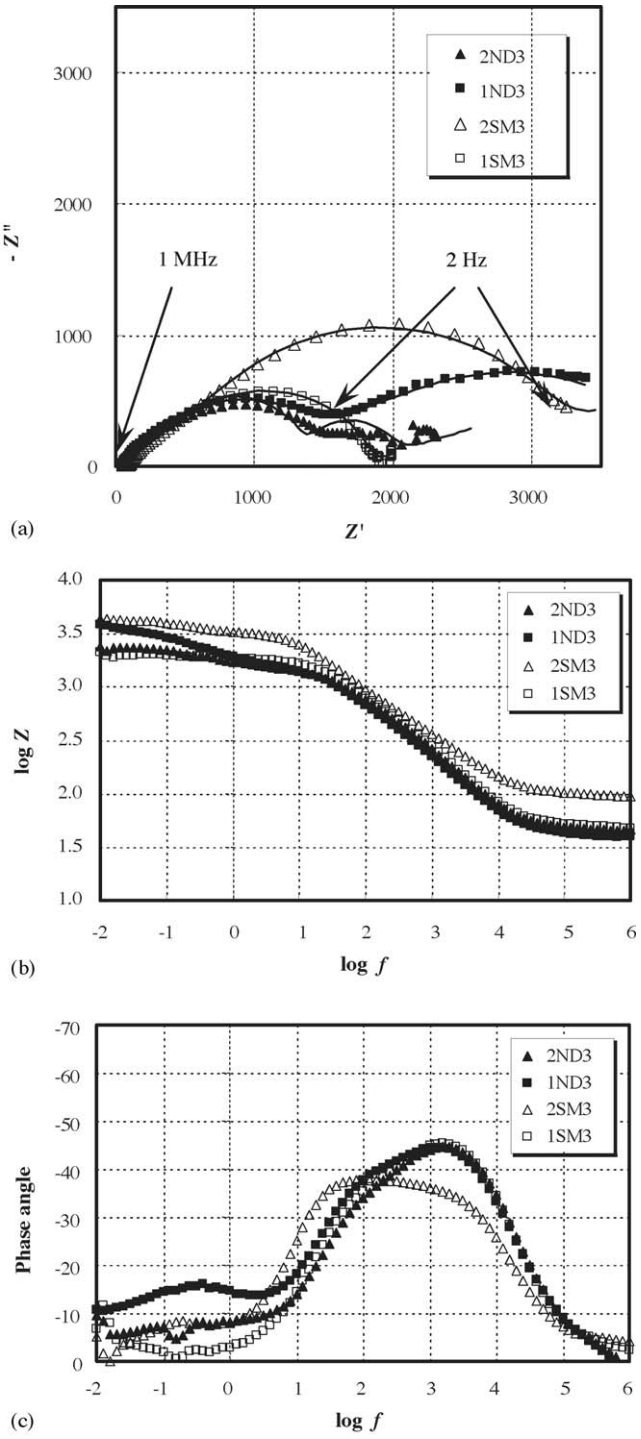

Fig. 4. (a–c) Nyquist plots and Bode plots for graphite/polysiloxane-based electrolyte/lithium metal cell measured at 0.5 V with various types of siloxane molecular structure having spacer (CH_2 group) or not, and different number of ethylene oxide.

The circuit parameters corresponding to the passive films were evaluated to clarify the dependence on cell voltage. The dependence of R_{film} for W100, 2ND3, and 1ND3 on cell voltage is shown in Fig. 6a to clarify the effect of numbers of silicon atoms and EO groups in the siloxane molecule. The number of silicons in the siloxane molecule affected the cell voltage dependency of R_{film}. The R_{film} increased between 1.7 and 1.8 V

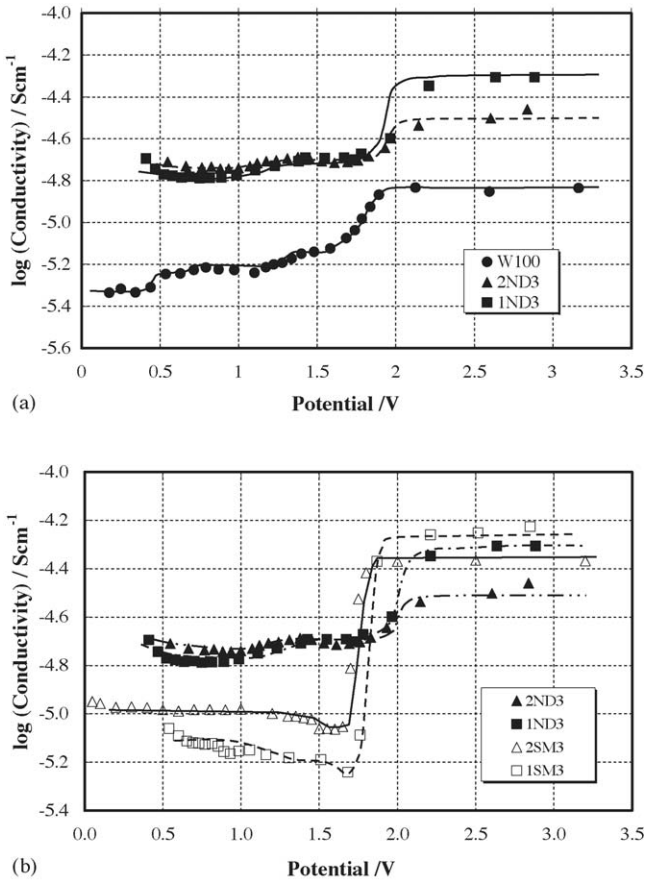

Fig. 5. The calculated conductivity of system as a function of the cell voltage: (a) effect of number of Si and (b) effect of spacer (CH_2 group) and number of ethylene oxide group.

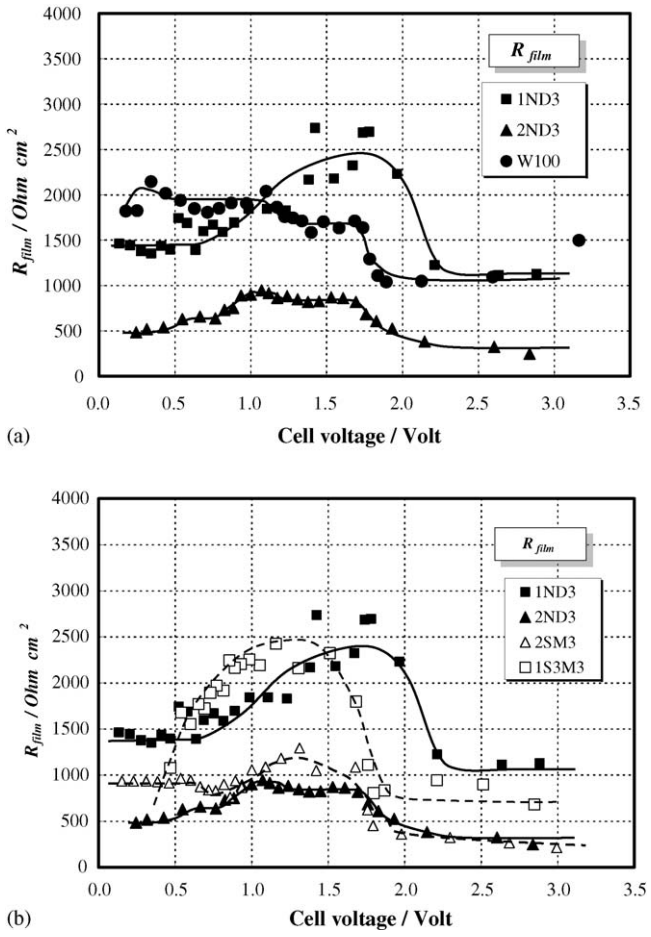

Fig. 6. Values of R_{film} as a function of the voltage of the graphite/polysiloxane-based electrolyte/lithium metal cell: (a) effect of number of Si and (b) effect of spacer (CH_2 group) and number of ethylene oxide group.

for W100, between 1.9 and 2 V for 2ND3, and between 1.7 and 2.2 V for 1ND3 as cell voltage decreased. Further increases in the R_{film} were observed between 1.2 and 1.4 V for W100, and between 1.1 and 1.3 V for 2ND3 with decrease of cell voltage. However, no secondary increase of the R_{film} was observed for 1ND3. The magnitude of R_{film} for 2ND3 was the smallest among these three electrolytes.

The effect of a functional group (spacer group and EO side chain) attached to a siloxane molecule can be seen in Fig. 6b, which shows the dependence of R_{film} on cell voltage for 2ND3, 2SM3, 1ND3, and 1S3M3. The cell voltage dependencies can be grouped according to the number of silicons, rather than the presence or absence of a spacer group or number of functional groups attached to the siloxane molecule. The R_{film} values for all electrolytes were constant above 2.2 V. The R_{film} for the siloxane containing only one silicon showed a maximum between 1.2 and 1.8 V. The R_{film} for the siloxane with two silicons showed two plateau regions—one below 0.5 V and one above 2.0 V. The dependency on cell voltage was significantly different from that of the 1-silicon siloxanes. The R_{film} for 2SM3 increased between 1.3 and 2.0 V, and decreased between 0.8 and 1.3 V with lower cell voltage. Unlike other electrolytes, the R_{film} for 2SM3 and 1ND3 was constant below 0.8 V.

The dependence of the charge transfer resistance, R_{ct}, on the cell voltage is shown in Fig. 7a for W100, 2ND3, and 1ND3. The objective was to clarify the effect of the number of silicons and the EO side chain groups on R_{ct}. The dependency of R_{ct} differed depending on the number of silicon atoms. The R_{ct} for all siloxanes showed constant values above 2.2 V. However, the R_{ct} for W100 increased drastically between 1.7 and 1.9 V, and monotonously between 0.5 and 1.7 V with decreasing cell voltage. The R_{ct} for 2ND3 and 1ND3 showed a maximum at 1.8 V, and then decreased.

The effect of a functional group in the siloxane molecule is revealed in Fig. 7b, which shows the dependence of R_{ct} for 2ND3, 2SM3, 1ND3, and 1S3M3 on the cell voltage. The functional group affected the dependence of R_{ct} on cell voltage. The R_{ct} for 2SM3 and 1S3M3, both of which contained a spacer group and fewer EO side chains, showed a maximum at 1.7–2 V and a minimum at 1–1.1 V.

5. Discussion

In earlier work, the morphological, compositional, and electrochemical characteristics of the graphite electrode surface charged in polysiloxane-based electrolyte with LiBOB were reported [17–20]. These investigations revealed the formation of island- and gel-like films, and indicated that the graphite

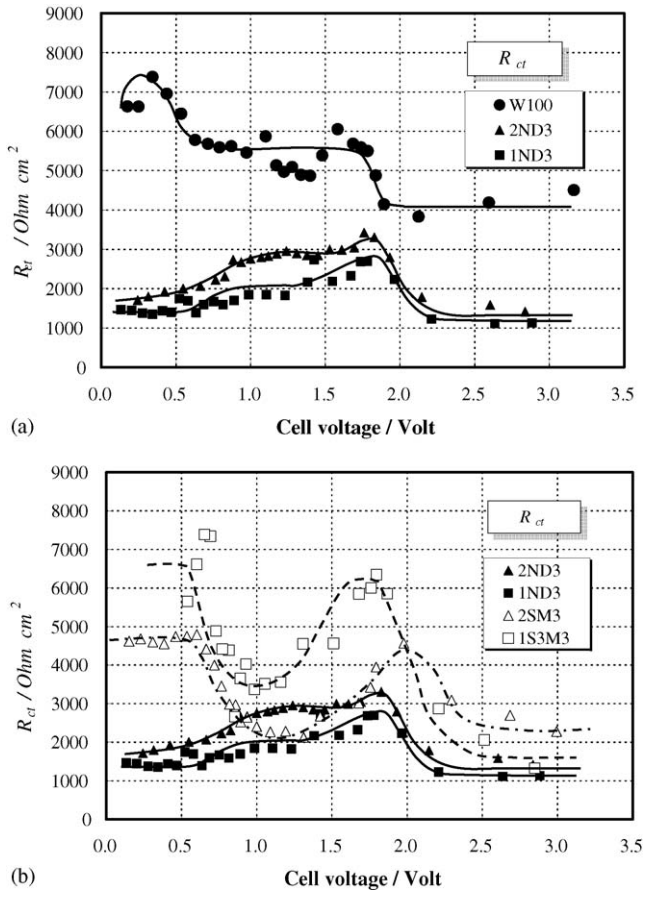

Fig. 7. Values of R_{ct} as a function of the voltage of graphite/polysiloxane-based electrolyte/lithium metal cell: (a) effect of number of Si and (b) effect of spacer (CH_2 group) and number of ethylene oxide group.

surface could be reformed by changing the electrolyte salt or by electrolyte additives [17–20]. Those results led to expectations that improvements in the siloxane-based electrolyte could support commercialization efforts in the lithium battery industry [19,20].

Previous reports indicated that preventing the formation of the gel-like film (Fig. 2b) was necessary to commercialize a siloxane electrolyte for use in lithium batteries [19,20]. In the present work, SEM images of the HOPG surface indicated that during charging in the 2SM3 electrolyte, less material was deposited and no gel-like film formed (Fig. 2g). The absence of this morphological feature suggests a large discharge capacity for the graphite electrode [19,20]. Electrolyte 2SM3 also produced an HOPG surface morphology similar to that produced in conventional carbonate electrolyte. Furthermore, close inspection of SEM images revealed that gel-like material deposited on the island-like film on the edge plane, although the gel-like film did not form on the basal plane.

The presence of gel-like material on edge planes is consistent with the compositional analysis, which showed higher concentrations of silicon and oxygen on edge planes than on the basal plane (Table 2). The gel-like film is produced by the decomposition of siloxane molecules [17–20]. The oxygen and silicon on the edge planes originate from the bis-oxalato borate anion and siloxane molecule, the decomposition of which was enhanced on the edge plane. This phenomenon is equivalent to the SEI formation for the carbonate electrolyte, which has been extensively reported [1–7]. The data summarized in Table 2 indicate that the 1ND3 electrolyte produced the least decomposition in the group of siloxanes without spacer groups, and that the 2SM3 electrolyte produced the least decomposition among those *with* a spacer group. In terms of the morphological and compositional features of the graphite surface, 1ND3 or 2SM3 are the most suitable siloxane electrolytes for commercialization. These electrolytes suppress island-like film formation on basal planes and reduce the extent of siloxane decomposition on edge planes.

Values of system conductivity shown in Fig. 5 at about 3 V before the first lithiation of the graphite electrode correspond to the electrolyte conductivity. For all siloxane electrolytes, the magnitude of the conductivity of system at 0.5 V and the degree of conductivity decrement, δ, between 0.5 and 3 V are summarized in Table 3. The magnitude of electrolyte conductivity at 3 V (Fig. 5) was greater for siloxanes with lower numbers of silicon.

Using the metric of system conductivity after initial lithiation at 0.5 V (Fig. 5a and b), the system conductivity for the siloxane with 1 or 2 silicons was an order of magnitude greater than that of the siloxane with 10 silicons. Siloxanes with one or two silicons did not cause much difference in system conductivity for both groups with and without spacer group. In terms of system conductivity, the siloxane with 1 or 2 silicons is more suitable for use in lithium batteries than that with 10 silicons. Furthermore, the decrease in system conductivity was attributed primarily to the electric contact resistance among graphite particles. This contact

Table 3
Conductivity of system, R_{film}, and R_{ct} for the present siloxane electrolytes

	Conductivity[a] (S cm^{-1})	Conductivity[b] (S cm^{-1})	δ (conductivity) (S cm^{-1})	R_{film}[c] (Ω cm^2)	R_{ct}[c] (Ω cm^2)
W100	1.46×10^{-5}	4.62×10^{-6}	9.99×10^{-6}	2143	7382
2ND3	3.48×10^{-5}	2.68×10^{-5}	7.98×10^{-6}	485.8	1708
1ND3	4.94×10^{-5}	2.57×10^{-5}	2.37×10^{-5}	1464	1443
1NM3	6.94×10^{-5}	1.29×10^{-5}	5.65×10^{-5}	3570	477.4
2SM3	4.29×10^{-5}	1.12×10^{-5}	3.17×10^{-5}	935.2	4621
1S3M3	5.95×10^{-5}	8.70×10^{-6}	5.08×10^{-5}	1078	6613

[a] Conductivity above 2.5 V.
[b] Conductivity below 0.5 V.
[c] Below 0.5 V.

resistance arose from the formation of passive films, because the voltage at which the conductivity decreased corresponded to the increase in film resistance, R_{film}. The conductivity decrease, δ, among siloxanes with a spacer group was significantly larger than that without the spacer group (Fig. 5b; Table 3).

Generally, the dependency of R_{film} on cell voltage was more affected by the number of silicons than by the presence or absence of spacer groups or number of functional groups (Fig. 6). In contrast, the dependency of R_{ct} on cell voltage was more affected by the latter than the former (Fig. 7). The R_{film} and R_{ct} values for all siloxane electrolytes are summarized in Table 3 for convenient comparisons. The siloxane with the smaller number of silicons provided the smaller R_{ct} (Fig. 7a). The R_{ct} for the siloxane with no spacer groups or more functional group was smaller than that with spacer groups or less functional group below 0.8 V (Fig. 7b). The reductions in R_{ct} below 0.8 V were attributed to the absence of spacer groups and/or the smaller number of functional groups (Fig. 7b). In the voltage region between 0.02 and 0.5 V, the R_{film} and the R_{ct} values for the 2SM3 and 1ND3 electrolytes were constant. The constant resistance values indicate that the passive film generated from these electrolytes complies with the morphological stresses generated by the volumetric expansion of graphite particles during lithiation. Hence, this quality of the passive film prevents the exposure of fresh graphite surface where the electrolyte is decomposed continuously. Furthermore, because the R_{film} of 2SM3 is less than that of 1ND3, the 2SM3 electrolyte is the best candidate for use in lithium battery among the present siloxane-based electrolytes.

Different molecular types of siloxane electrolyte in lithium secondary electrochemical cells (lithium transition metal oxide cathode and graphite anode) were evaluated by long-term testing, such as cycling and calendar life [67]. In previous work, the 2SM3 electrolyte showed the greatest discharge capacity retention after long-term testing, including cycling and calendar life tests [67], a finding that is consistent with conclusions of the present investigation. Interpretations of test results led to the hypotheses that the elastic passive film formed by the decomposition of 2SM3 on the graphite surface, and that the superior passive film prevented siloxane-based electrolyte from continuous decomposition under long-term testing conditions. The present study also led to the assertion that the compounds might be comprised of –Si–O– bonding or –C–O– bonding that rotates in unconstrained fashion to absorb the volumetric change of graphite during charge–discharge cycling. The characterization of molecular structure of the SEI film is beyond the scope of the present study.

6. Conclusions

The characteristics of passive films formed on a graphite electrode were modified by changing the molecular structure of the siloxane. The 2SM3 siloxane electrolyte exhibited the strongest tendency to inhibit passive film formation on HOPG, and showed the lowest concentrations of silicon and oxygen on edge planes.

The 2SM3 electrolyte exhibited a large conductivity *decrement* (δ) at 1.7–1.8 V, and low system conductivity below 0.5 V. These values must be improved for practical use in lithium batteries. Recent investigations of the polysiloxane-based electrolyte with an additive [19] and with a modified electrolyte salt [20] illustrate possible pathways for improvements required for development of a lithium battery for practical use.

The voltage range below ~0.5 V is close to the actual operating range for lithium batteries, and in this range, the magnitude of R_{ct} for 2SM3 was 4621 $\Omega\,cm^2$. This value of R_{ct} is two orders of magnitude greater than conventional carbonate-based electrolytes, such as the ones containing $LiPF_6$ (3–10 $\Omega\,cm^2$ [34]) and $LiClO_4$ (60–80 $\Omega\,cm^2$ [46]). However, the R_{film} and R_{ct} values for the 2SM3 and 1ND3 electrolytes did not show a dependence on cell voltage at 0.02–0.5 V. Furthermore, the passive film on the graphite electrode is composed of compounds including flexible –Si–O– and –C–O– bonding on the graphite electrode. From these observations, we conclude that in the 2SM3 and 1ND3 electrolytes, elastic passive films are formed that prevents continuous decomposition of the siloxane electrolyte on the graphite surface. The long-term battery performance, such as cycle life and calendar life, is expected to be superior in a battery containing a 2SM3 siloxane electrolyte because of the formation of an elastic passive film on the graphite electrode. The passive film prevents continuous decomposition of the electrolyte by the exposed graphite due to the graphite expansion and shrinkage during lithiation and delithiation. In future work, the 2SM3 siloxane electrolyte will be modified with dissolving organo-borate salts and electrolyte additives, and the resulting battery performance will be investigated and developed for future use in the lithium battery industry.

Acknowledgements

Support from the US Army Communications-Electronics Command Center (CECOM), University of Wisconsin, and Argonne National Laboratory is gratefully acknowledged. Helpful suggestions with Prof. F. Mansfeld are also acknowledged.

References

[1] M. Inaba, Z. Shiroya, Y. Kawatate, A. Funabiki, Z. Ogumi, J. Power Sources 68 (2) (1997) 221–226.
[2] S.-K. Jeong, M. Inaba, Y. Iriyama, T. Abe, Z. Ogumi, Electrochim. Acta 47 (2002) 1975–1982.
[3] R. Mogi, M. Inaba, Y. Iriyama, T. Abe, Z. Ogumi, J. Power Sources 108 (2002) 163–173.
[4] D. Aurbach, E. Zinigrad, Y. Cohen, H. Teller, Solid State Ionics 148 (2002) 405–416.
[5] D. Aurbach, I. Weissman, A. Zaban, P. Dan, Electrochim. Acta 45 (1999) 1135–1140.
[6] D. Aurbach, A. Zaban, Y. Gofer, Y.E. Ely, I. Weissman, O. Chusid, O. Abramson, J. Power Sources 54 (1995) 76–84.
[7] Z. Ogumi, A. Sano, M. Inaba, T. Abe, J. Power Sources 97–98 (2001) 156–158.
[8] K. Xu, S. Zhang, B.A. Poese, T.R. Jow, Electrochem. Solid-State Lett. 5 (1) (2002) A259–A262.
[9] K. Xu, S. Zhang, T.R. Jow, W. Xu, C.A. Angell, Electrochem. Solid-State Lett. 5 (1) (2002) A26–A29.
[10] K. Xu, S. Zhang, T.R. Jow, Electrochem. Solid-State Lett. 6 (6) (2003) A117–A120.

[11] Y. Kang, W. Lee, D.H. Suh, C. Lee, J. Power Sources 119–121 (2003) 448–453.
[12] I.J. Lee, G.S. Song, W.S. Lee, C. Lee, J. Power Sources 114 (2003) 320–329.
[13] M. Shibata, T. Kobayashi, R. Yosomiya, M. Seki, Eur. Polym. J. 36 (2000) 485–490.
[14] Z. Zhang, S. Fang, Electrochim. Acta 45 (2000) 2131–2138.
[15] Z. Wang, M. Ikeda, N. Hirata, M. Kubo, T. Ito, O. Yamamoto, J. Electrochem. Soc. 146 (6) (1999) 2209–2215.
[16] B. Oh, D. Vissers, Z. Zhang, R. West, H. Tsukamoto, K. Amine, J. Power Sources 119–121 (2003) 442–447.
[17] H. Nakahara, A. Masias, S.Y. Yoon, T. Koike, K. Takeya, Proceedings of the 41st Power Sources Conference in Philadelphia, June 14–17, 2004, p. 165.
[18] H. Nakahara, S.Y. Yoon, T. Piao, S. Nutt, F. Mansfeld, J. Power Sources, in press.
[19] H. Nakahara, S.Y. Yoon, S. Nutt, J. Power Sources, in press.
[20] H. Nakahara, S. Nutt, J. Power Sources, in press.
[21] N. Hiroyoshi, S. Kuroiwa, H. Miki, M. Tsunekawa, T. Hirajima, Hydrometallurgy 74 (2004) 193.
[22] K. Abe, H. Yoshitake, T. Kitakura, T. Hattori, H. Wang, M. Yoshio, Electrochim. Acta 49 (26) (2004) 4613–4622.
[23] M.-S. Wu, P.-C.J. Chiang, J.-C. Lin, J.-T. Lee, Electrochim. Acta 49 (2004) 4379.
[24] M.S. Michael, S.R.S. Prabaharan, J. Power Sources 136 (2004) 250.
[25] S.-H. Choi, J. Kim, Y.-S. Yoon, Electrochim. Acta 50 (2–3) (2004) 547.
[26] C.H. Chen, J. Liu, M.E. Stoll, G. Henriksen, D.R. Vissers, K. Amine, J. Power Sources 128 (2004) 278.
[27] J.-H. Kim, C.W. Park, Y.-K. Sun, Solid State Ionics 164 (2003) 43.
[28] Z.P. Guo, S. Zhong, G.X. Wang, H.K. Liu, S.X. Dou, J. Alloys Compd. 348 (2003) 231.
[29] S.S. Zhang, T.R. Jow, J. Power Sources 109 (2002) 458.
[30] S. Zhang, P. Shi, Electrochim. Acta 49 (2004) 1475.
[31] Z. Ogumi, T. Abe, T. Fukutsuka, S. Yamate, Y. Iriyama, J. Power Sources 127 (2004) 72.
[32] S. Komaba, T. Itabashi, B. Kaplan, H. Groult, N. Kumagai, Electrochem. Commun. 5 (2003) 962.
[33] J. Yao, G.X. Wang, J.-H. Ahn, H.K. Liu, S.X. Dou, J. Power Sources 114 (2004) 292.
[34] M. Nookala, B. Kumar, S. Rodrigues, J. Power Sources 111 (2002) 165.
[35] Y.-K. Choi, K.-I. Chung, W.-S. Kim, Y.-E. Sung, S.-M. Park, J. Power Sources 104 (2002) 132.
[36] S.B. Lee, S.-I. Pyun, Carbon 40 (2002) 2333.
[37] A.M. Andersson, Dissertation for the Degree of Doctor of Philosophy in Uppsala University in 2001.
[38] G. Eichinger, J. Electroanal. Chem. 74 (1976) 183.
[39] J.O. Besenhard, Carbon 14 (1976) 111.
[40] D. Aurbach, Nonaqueous Electrochemistry, Marcel Dekker, New York, 1999.
[41] D. Aurbach, A. Zaban, Y. Ein-Eli, I. Weissman, O. Chusid, B. Markovsky, M. Levi, A. Shechter, E. Granot, J. Power Sources 68 (1997) 91.
[42] M. Ue, M. Takeda, M. Takehara, S. Mori, J. Electrochem. Soc. 144 (1997) 2684.
[43] H. Nakahara, Study of passive film formation on graphite surface in polysiloxane-based electrolyte for the application of Li secondary battery, Ph.D. Dissertation, University of Southern California, 2006.
[44] C.S. Wang, A.J. Appleby, F.E. Little, Electrochim. Acta 46 (2001) 1793.
[45] B. Jin, J.-U. Kim, H.-B. Gu, J. Power Sources 117 (2003) 148.
[46] C.R. Yang, J.Y. Song, Y.Y. Wang, C.C. Wan, J. Appl. Electrochem. 30 (2000) 29.
[47] Y.C. Chang, J.H. Jong, G.T.K. Fey, J. Electrochem. Soc. 147 (2000) 2033.
[48] Y.C. Chang, H.J. Sohn, J. Electrochem. Soc. 147 (2000) 50.
[49] M. Holzapfel, A. Martinent, F. Alloin, B. Le Gorrec, R. Yazami, C. Montella, J. Electroanal. Chem. 546 (2003) 41.
[50] T. Piao, S.M. Park, C.H. Doh, S.I. Moon, J. Electrochem. Soc. 146 (1999) 2794.
[51] F. Prieto, I. Navarro, M. Rueda, J. Electroanal. Chem. 550–551 (2003) 253.
[52] N. Hiroyoshi, S. Kuroiwa, H. Miki, M. Tsunekawa, T. Hirajima, Hydrometallurgy 74 (2004) 193.
[53] S. Yoon, H. Kim, S.-M. Oh, J. Power Sources 94 (2001) 68.
[54] J.R. MacDonald, Impedance Spectroscopy: Emphasizing Solid Materials and Systems, John Wiley & Sons, New York, 1987.
[55] J. Bisquert, A. Compte, J. Electroanal. Chem. 499 (2001) 112.
[56] Y.O. Kim, S.M. Park, J. Electrochem. Soc. 148 (2001) A194.
[57] E. Basrsoukov, J.H. Kim, C.H. Yoon, H. Lee, J. Electrochem. Soc. 145 (1998) 2711.
[58] J.-S. Kim, Y.-T. Park, J. Power Sources 91 (2000) 172.
[59] M.W. Wagner, Electrochim. Acta 10 (1997) 1623.
[60] V. Doge, J. Dreher, G. Hambitzer, IEEE 0-7803-2459-5/95 (1995).
[61] S. Buller, M. Thele, R.W. De Doncker, IEEE 0-7803-0/03 (2003).
[62] I. Uchida, M. Mohamedi, K. Dokko, M. Nishizawa, T. Itoh, M. Umeda, J. Power Sources 97–98 (2001) 518.
[63] R.M. Spotnitz, IEEE 0-7803-5924-0/00 (2000).
[64] M.J. Issacson, N.A. Torigoe, R.P. Hollandsworth, IEEE 0-7803-4098-1/98 (1998).
[67] S.-Y. Yoon, H. Nakahara, Z. Zhang, Q. Wang, K. Amine, R. West, H. Tsukamoto, Proceedings of the 2nd International Conference on Polymer Batteries and Fuel cells, Las Vegas, USA, June 12–17, 2005 (Abstract No. 121).